5
Measurement of the Solid-Liquid Interface Energy in Ternary Alloy Systems

Annemarie Bulla, Emir Subasic, Ralf Berger, Andreas Bührig-Polaczek, and Andreas Ludwig

5.1
Introduction

The aim of this chapter is to point out a methodology to determine the solid–liquid interface energy in binary and ternary alloy systems. The solid–liquid interface energy, σ_{SL}, is defined as reversible work required for creating a unit area of the interface at constant temperature, volume, and chemical potentials and is of major importance during phase transformation that is phase nucleation, crystal growth, and the final grain structure. In addition to chemical diffusion, this quantity governs the microstructural length scale of solidification morphologies. Therefore, the solid–liquid interface energy is an important parameter in many analytical and numerical models of solidification and ripening. The measurement of the solid–liquid interface energy is very difficult. For binary alloys, the literature provides only limited experimental data, and ternary alloys have been analyzed for the first time in the present study.

One of the most common experimental techniques for measuring the solid–liquid interface energy is the "grain boundary groove in an applied temperature gradient" method [1–18]. To measure the solid–liquid interface energy, a radial heat flow apparatus was constructed and assembled as described by Gündüz [11]. After the equilibration process, the samples were metallographically investigated and the local curvature of the grooves was analyzed. The interface energy was obtained using the Gibbs–Thomson equation, which requires measuring the local curvature of the grain boundary grooves, determining the local undercooling by heat flux simulations, and calculating the entropy of fusion to obtain the solid–liquid interface energy.

In the present chapter, the radial heat flow apparatus was applied to reproduce previous results for a eutectic Al–Cu alloy and to measure the solid–liquid interface energy for an alloy with invariant eutectic composition in the ternary system Al–Cu–Ag. In order to describe the influence of concentration on the solid–liquid interface energy, additional experiments were carried out.

Phase Transformations in Multicomponent Melts. Edited by D. M. Herlach

ISBN: 978-3-527-31994-7

5.2
Experimental Procedure

5.2.1
The Radial Heat Flow Apparatus

On the basis of the work of Gündüz [11] a radial heat flow apparatus for measuring the solid–liquid interface energy was assembled as shown in Figure 5.1. Because of its axial symmetry the apparatus allows a stable temperature gradient to be maintained, using a single heating wire emitting a power of P over a length of l along the axis of a cylindrical sample, and a water cooled jacket at the outside of the sample.

According to Fourier's law (provided a constant radial heat flux)

$$\dot{Q} = -\lambda 2\pi r l \frac{dT}{dr} \quad \text{with} \quad P = \frac{Q}{t} = \dot{Q} \tag{5.1}$$

where λ (W K^{-1}.m) is the thermal conductivity which is material dependent. The Equation 5.1 may be integrated as follows:

$$\dot{Q} = \frac{-\lambda 2\pi l(T_2 - T_1)}{\ln\left(\frac{r_2}{r_1}\right)} \tag{5.2}$$

where T_1 and T_2 are the temperatures at r_1 and r_2, respectively. The temperature gradient G_S at r required for the measurement of σ_{SL} could be determined by measuring the temperatures T_1 and T_2, respectively.

$$G_S = -\frac{\dot{Q}}{2\pi r l \lambda} \tag{5.3}$$

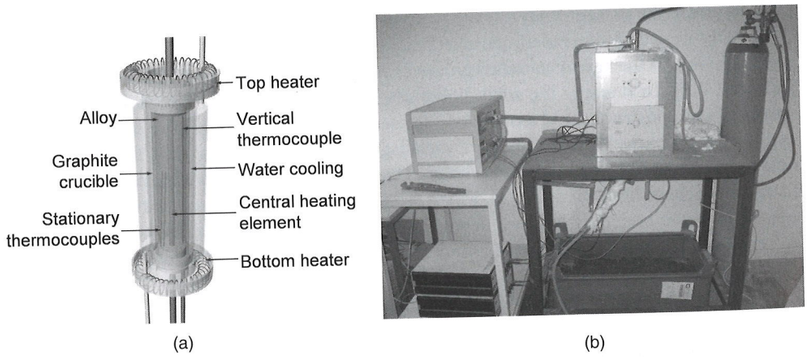

Fig. 5.1 (a) Schematic illustration of the radial heat flow apparatus. (b) The whole assembly of the radial heat flow apparatus.

5.2.2
Equilibration of the Sample

During the equilibration process, the sample was heated at the center using the central heating element and cooled on the outside using the water cooling jacket to establish a stable radial temperature gradient. This was ensured by a temperature controller using calibrated thermocouples. The top and bottom heaters were adjusted so that the vertical isotherms run parallel to the central axis. To prevent a horizontal convectional flow, only a thin liquid layer (1–2 mm thick) was melted along the ceramic tube surrounding the central heating element. The semisolid samples were held in a stable radial temperature gradient for about 2–4 days—depending on the alloy—until a dynamic balance has been reached in which the solid–liquid interface has stabilized in a constant temperature field. During the annealing, the mean temperature deviation was about ±0.02 °C in 1 h and ±0.05 °C in 2 days.

5.2.3
Quenching

The shape of the cusps had to be preserved by rapid quenching. This was realized by turning off the input power to all heaters. Figure 5.2 shows the temperature versus time plot during quenching. At the beginning of the quenching process, the cooling rate at the thermocouples was approximately 40 °C min^{-1}.

5.3
Evaluation of the Local Curvature of the Grain Boundary Grooves

5.3.1
Preparation of the Sample

The cylindrical samples were cut in a transverse direction in 20 mm slices and metallographically prepared. The microexamination of the samples was done using

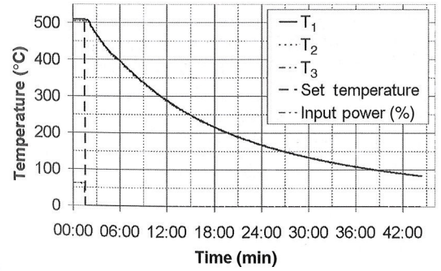

Fig. 5.2 Rapid quenching of the sample achieved by turning off the input power.

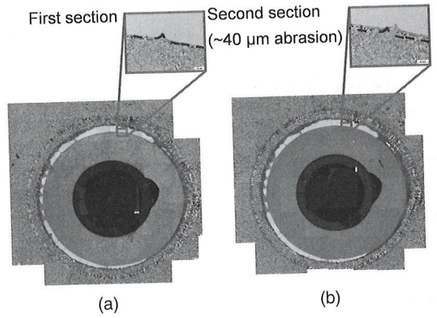

Fig. 5.3 Two cross sections of a specimen with a defined distance of a eutectic Al–Cu–Ag alloy consisting of 50 single pictures magnified 50 times: (a) first plane, (b) second plane.

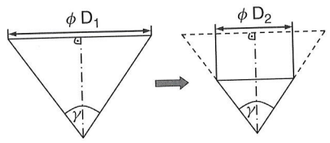

Fig. 5.4 Changes in the diameter of the central holes after grinding. The half angle at the tip of the drill bit, γ, was used to determine the amount of abrasion d, where D is the diameter of the drilled holes at the surface.

an optical light microscope. The grain boundary grooves were photographed at a magnification of 500, to allow an accurate measurement of the local curvature of the grooves. The x and y coordinates of the grain boundary grooves were determined using a computer-aided design (CAD) software. To determine the orientation of the grain boundary grooves relative to the polished surface, two cross-sectional cuts with a defined distance were required (Figure 5.3).

In order to determine the amount of abrasion, d, in the specimen, four opposite center holes were drilled into the polished surface with a drill bit angle of 90°. From the variation in the diameter, the amount of abrasion was calculated (Figure 5.4).

5.3.2 Geometrical Correction of the Groove Coordinates

To calculate the magnitude of the grain, it is assumed that no curvature exists along the direction of the cusp line (z direction) of the grain boundary groove. Owing to the translation invariance in this direction, the 3D geometry of the grain boundary groove can be reduced to a 2D one by a projection to a plane orthogonal to the cusp line. Since the polished surfaces of the specimens are not perpendicular to

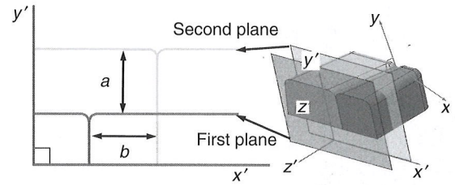

Fig. 5.5 Schematic drawing to show the relation between the coordinate systems of the grain and of the ground cross section [14].

the surfaces of the grain boundary groove (Figure 5.5), a transformation of the x and y coordinates of the grain boundary groove is necessary.

The coordinates of the cusps, x', y', from the metallographic section must be projected into an x- y-, z-coordinate system aligned with the grain. This new coordinate system is oriented such that the z axis is parallel to the base of the grain boundary groove and the y axis is perpendicular to the macroscopic solid–liquid interface plane. The measured x', y' coordinates are then projected onto the $z = 0$ plane in the coordinate system of the grain. The transformation can be expressed as follows:

$$x = x' \frac{\sqrt{a^2 + d^2}}{\sqrt{a^2 + b^2 + d^2}} + y' \frac{-ab}{\sqrt{a^2 + d^2}\sqrt{a^2 + b^2 + d^2}} \tag{5.4}$$

$$y = y' \frac{d}{\sqrt{a^2 + d^2}} \tag{5.5}$$

and

$$d = \frac{D_1 - D_2}{2 \tan \gamma} \tag{5.6}$$

5.3.3 Determination of the Local Undercooling

If the solid and liquid phases have different thermal conductivities, the isotherms at the grain boundary groove cusps are deformed and the local undercooling has to be determined numerically. Figure 5.6 shows an example of a numerical simulation of the microscopic temperature field, to determine the local deformation of the isotherms at the grain boundary groove.

The shape of the solid–liquid interface was extrapolated using the transformed experimental groove shape. Fixed temperatures have been set at the bottom and the top of the domain, deduced from the macroscopic temperature gradient measured during the equilibration experiment. On either side of the domain the lateral heat flux is zero. The temperature field simulations were carried out using the commercial software FLUENT. To automate the calculation of the local undercooling,

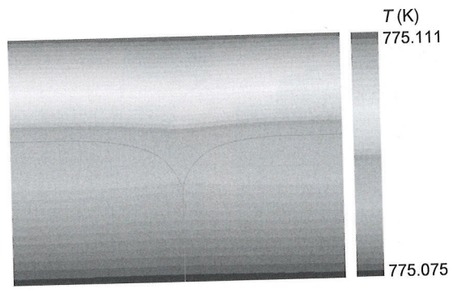

Fig. 5.6 Numerically determined temperature distribution at a grain boundary groove in an Al–Cu–Ag alloy.

a suitable program code was developed that quantifies the undercooling along a grain boundary groove in order to calculate the Gibbs–Thomson coefficient.

5.3.4
Determining the Interface Energy

On the basis of the two-dimensional geometry of the grain boundary groove obtained by the coordinate transformation (Section 3.2) the Gibbs–Thomson equation at any point of the curve of the grain boundary groove could be expressed as follows:

$$\Delta T_r = \frac{\Gamma}{r} \tag{5.7}$$

where r is the radius of the curvature at this point. Since measurement errors could lead to large inaccuracies in the determination of the curvature, the Gibbs–Thomson equation was not evaluated directly but in an integral form as shown below:

$$\int_{y_1}^{y_n} \Delta T_r \mathrm{d}y = \Gamma \int_{y_1}^{y_n} \frac{1}{r} \mathrm{d}y \tag{5.8}$$

The left hand side of the equation was evaluated numerically, determining the appropriate undercooling, ΔT_r, at a point, y_n, in the simulated temperature field.

$$\int_{y_1}^{y_n} \Delta T_r \mathrm{d}y \approx \sum_{i=1}^{n-1} (y_i - y_{i+1}) \left(\frac{\Delta T_i + \Delta T_{i+1}}{2} \right) \tag{5.9}$$

The right-hand side of Equation 5.8 may be evaluated for any shape by setting the length element $\mathrm{d}s = r\,\mathrm{d}\theta$, where s is the distance along the interface and θ is the angle of a tangent to the interface with the y axis (Figure 5.7). Hence, $\mathrm{d}y = \cos(\theta)\,\mathrm{d}s = \cos(\theta) r \mathrm{d}\theta$ can be substituted on the right-hand side of Equation 5.8

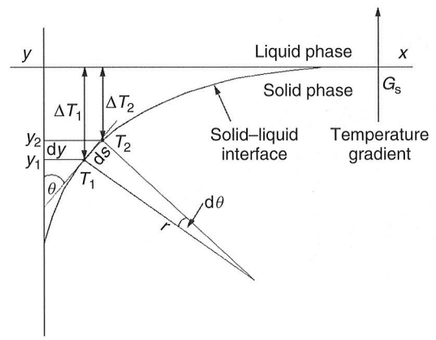

Fig. 5.7 Temperature difference at two different points of the grain boundary groove and description of ds, dθ, and r.

which is as follows for an arbitrary surface:

$$\Gamma \int_{y_1}^{y_n} \frac{1}{r} \mathrm{d}y = \Gamma \int_{\theta_1}^{\theta_n} \frac{1}{r} r \cos(\theta) \mathrm{d}\theta = \Gamma (1 - \sin\theta) \Big|_{\theta_1}^{\theta_n} = \Gamma(\sin\theta_1 - \sin\theta_n) \tag{5.10}$$

This allows the Gibbs–Thomson coefficient to be calculated by numerically evaluating the right-hand side of Equation 5.8 using the undercooling temperatures from temperature field simulations and measuring the angle θ by constructing a tangent to the surface at y_n. The solid–liquid interface energy is obtained from the definition of the Gibbs–Thomson coefficient:

$$\Gamma = \frac{\sigma_{SL}}{\Delta S^*} \tag{5.11}$$

ΔS^* is the specific entropy change per unit volume at transformation temperature, which must be known or obtained from other sources. In this study, the entropy has been determined by Thermo-Calc using the database described by Witusiewicz *et al.* [19].

5.4
Results and Discussion

The described procedure was tested to reproduce previous results obtained by Gündüz [11, 12] and Maraşli [14, 15] for a binary Al–Cu alloy with a eutectic composition. Afterwards, the solid–liquid interface energy was measured for the first time for an alloy with an invariant eutectic composition in the ternary system Al–Cu–Ag. The used alloy had a eutectic composition of 16.86 wt% Cu and 39.97 wt% Ag at a temperature of 502 °C. In order to describe the influence of the concentration on the solid–liquid interface energy, further experiments were

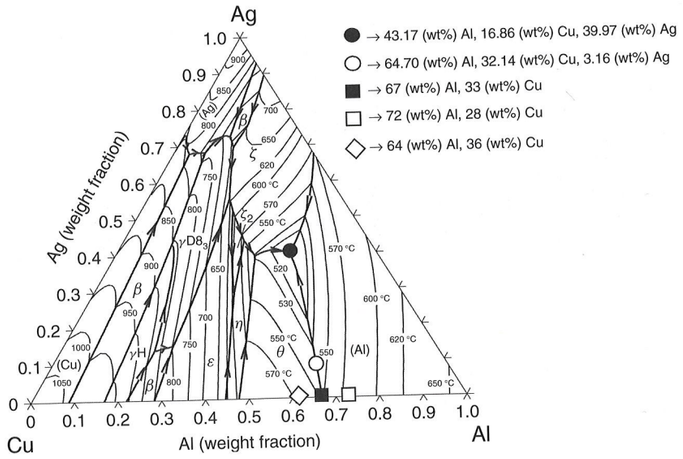

Fig. 5.8 Projection of the liquid surfaces with isothermals plotted in the different phase regions of the Al–Cu–Ag system, with the examined alloys.

carried out for binary Al–Cu alloys adjacent to the Al–Cu alloy with eutectic composition using samples with 28 and 36 wt% Cu, respectively. Furthermore, the solid–liquid interface energy was calculated for an Al–Cu–Ag alloy with a monovariant composition. In Figure 5.8 the examined alloys are displayed.

5.4.1
Al–Cu System with Eutectic Composition

Figure 5.9 shows grain boundary groove shapes of the $Al_{(\alpha)}$ and $CuAl_2$ phase in equilibrium with the quenched liquid and the temperature field simulation of these grains (Figure 5.9a and b). The samples were left in the radial heat flow apparatus for two days until the grain boundary grooves were equilibrated. After quenching, the samples were metallographically prepared and analyzed. An average value of the Gibbs–Thomson coefficient for the solid $Al_{(\alpha)}$–liquid Al–Cu system was found to be $\Gamma = 28 \pm 7 \times 10^{-8}$ K m. With a specific entropy change per unit volume of $\Delta S^* = 6.78 \times 10^5$ J m^{-3} K [14] a solid–liquid interface energy of $\sigma_{SL} = 190 \pm 48$ mJ m^{-2} was calculated. The relative error for the solid–liquid interface energy was about 25%. The small amount of abrasion in this experiment ($\bar{d} = 6.9\,\mu$m) has led to large inaccuracies for the geometrical transformations and hence to the curvature of the grain boundary groove shapes as well as the simulated temperatures.

The evaluation of the solid $CuAl_2$–liquid Al–Cu phase gave an average value of $\Gamma = 5.0 \pm 0.9 \times 10^{-8}$ K m for the Gibbs–Thomson coefficient. The solid–liquid interface energy, σ_{SL}, was found to be 80 ± 15 mJ m^{-2} with a specific entropy

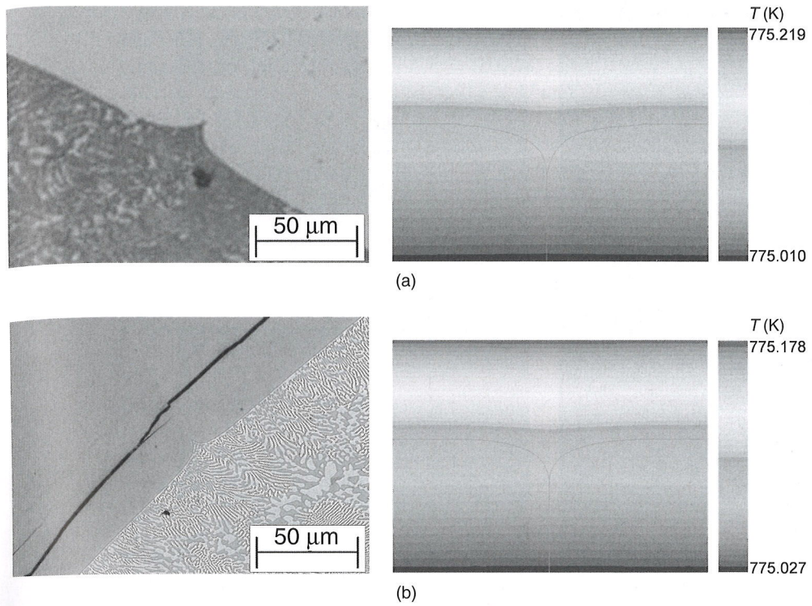

Fig. 5.9 Grain boundary groove shapes of the phases in equilibrium with the quenched liquid. (a) $Al_{(\alpha)}$ phase and (b) $CuAl_2$ phase in equilibrium with the quenched liquid.

change per unit volume of $\Delta S^* = 15.95 \times 10^5$ J m^{-3} K [14]. A relative error of 18% for the solid–liquid interface energy was calculated. The comparison of the average value of the solid–liquid interface energy of the $Al_{(\alpha)}$ and $CuAl_2$ phases shows that within the margin of error, the values of σ_{SL} were in a good accordance with previous results of Gündüz [11, 12] and Maraşli [14, 15].

5.4.2
Al–Cu–Ag System with Invariant Eutectic Composition

Further experiments were carried out to determine the solid–liquid interface energy in the ternary Al–Cu–Ag system. The samples were left in the radial heat flow apparatus for 4 days maintaining a constant temperature gradient until the grain boundary grooves were in local equilibrium (Figure 5.10). The Gibbs–Thomson coefficient was calculated for each phase. For numerical determination of the local undercooling, the thermal conductivity of the solid phase was determined experimentally for each phase by means of the laser-flash method [20–22] and differential scanning calorimetry (DSC). The thermal conductivity of the liquid phase was

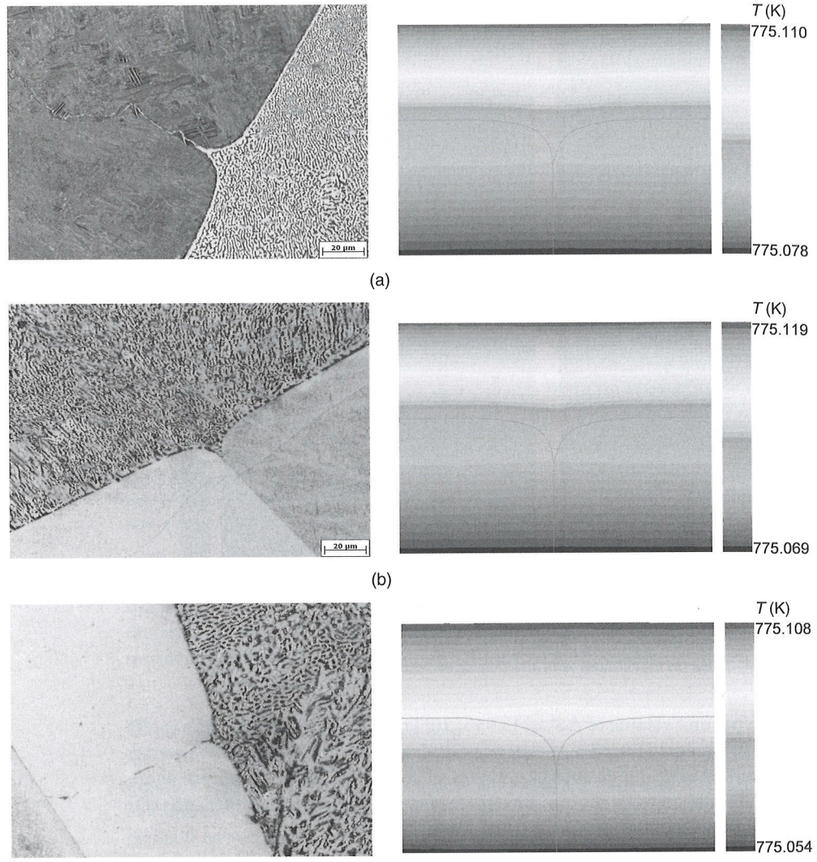

Fig. 5.10 Grain boundary groove shapes of the different phases in equilibrium with the quenched liquid. (a) $Al_{(\alpha)}$ in equilibrium with the quenched liquid; (b) $CuAl_2$ in equilibrium with the quenched liquid; (c) Ag_2Al in equilibrium with the quenched liquid.

determined experimentally by means of a unidirectional growth apparatus that is a Bridgman furnace. The average value of the Gibbs–Thomson coefficient for the solid $Al_{(\alpha)}$–liquid Al–Cu–Ag system was found to be $\Gamma = 4.8 \pm 0.7 \times 10^{-8}$ K m. With a specific entropy change per unit volume of $\Delta S^* = 10.75612 \times 10^5$ J m^{-3} K, the solid–liquid interface energy, σ_{SL}, was found to be 51 ± 8 mJ m^{-2}. The relative error was about 15%.

For the solid $CuAl_2$–liquid Al–Cu–Ag system, an average value of the Gibbs–Thomson coefficient of $\Gamma = 5.9 \pm 0.9 \times 10^{-8}$ K m was determined. With a specific entropy change per unit volume of $\Delta S^* = 18.88085 \times 10^5$ J m^{-3} K, the solid–liquid interface energy, σ_{SL}, was found to be 111 ± 17 mJ m^{-2}. The relative error was about 15%.

For the solid Ag_2Al–liquid Al–Cu–Ag system, the average value of the Gibbs–Thomson coefficient was found to be $\Gamma = 5 \pm 0.9 \times 10^{-8}$ K m. The solid–liquid interface energy, σ_{SL}, was found to be 59 ± 11 mJ m^{-2}. A specific entropy change per unit volume of $\Delta S^* = 11.70052 \times 10^5$ J m^{-3} K was calculated. The relative error was about 18%. Comparing the results of the solid–liquid interface energy for the $Al_{(\alpha)}$ phase shows that in the ternary system the value is about 2.5 times smaller than in the binary system, whereas the value for the $CuAl_2$ phase is in the same range.

5.4.3 Concentration Dependence of σ_{SL}

The radial heat flow apparatus was used to measure the solid–liquid interface energy in the binary Al–Cu system with 28 and 36 wt% Cu. In Table 5.1 the average values of the Gibbs–Thomson coefficient and the solid–liquid interface energy for the different phases of the alloys investigated are displayed.

For the sample Al–Cu28, an average value of the solid–liquid interface energy of 117 ± 14 mJ m^{-2} for the $Al_{(\alpha)}$ phase and 83 ± 12 mJ m^{-2} for $CuAl_2$ phase was calculated. For the sample Al–Cu36, the solid–liquid interface energy was found to be 216 ± 41 mJ m^{-2} for the $Al_{(\alpha)}$ phase and 214 ± 13 mJ m^{-2} for $CuAl_2$ phase. Comparing the results of the solid–liquid interface energy for the $CuAl_2$ phase shows that in the Al–Cu system with 28 wt% Cu the value was in good accordance with the results in the Al–Cu system with eutectic composition, whereas in the Al–Cu system with 36 wt% Cu the value was 2.5 times higher. For the determination of the concentration dependency of the solid–liquid interface energy in the Al–Cu–Ag system, a sample with 32.14 wt% Cu and 3.16 wt% Ag was used (Figure 5.8). For the $Al_{(\alpha)}$ phase an average value of the solid–liquid interface

Table 5.1 Results of the Gibbs–Thomson coefficient, Γ, and the solid–liquid interface energy, σ_{SL}, (a) Al—28 wt% Cu; (b) Al—36 wt% Cu; (c) Al—32.14 wt% Cu—3.16 wt% Ag.

Solid phase	$\Gamma \times 10^{-8}$ (K m)	σ_{SL} (mJ m^{-2})
(a) Alpha Al—7.68 wt% Cu	17 ± 2	117 ± 14
(a) Theta Al—55.09 wt% Cu	5.2 ± 0.8	83 ± 12
(b) Alpha Al—7.89 wt% Cu	32 ± 6	216 ± 41
(b) Theta Al—55.13 wt% Cu	13 ± 2	214 ± 13
(c) Alpha Al—7.87 wt% Cu—4.96 wt% Ag	14 ± 3	92 ± 17
(c) Theta Al—56.56 wt% Cu–0.29 wt% Ag	4.5 ± 0.9	84 ± 17

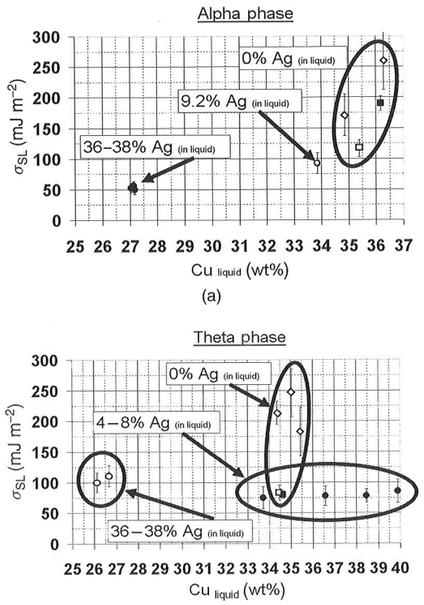

Fig. 5.11 Solid–liquid interface energy as a function of the copper concentration. (a) Alpha phase; (b) theta phase.

energy of 92 ± 17 mJ m^{-2} was calculated and for the $CuAl_2$ phase the solid–liquid interface energy was found to be 84 ± 17 mJ m^{-2}.

In Figure 5.11 the average values of the solid–liquid interface energy of the $Al_{(\alpha)}$ phase and the $CuAl_2$ phase with respect to the Cu concentration in the liquid phase are displayed. The comparison of the average value of the solid–liquid interface energy of the $Al_{(\alpha)}$ phase versus the concentration of Cu in the liquid phase shows that, within the margin of error, the solid–liquid interface energy increases with the concentration of Cu and decreases with increasing Ag concentration. A comparison of the average value of the solid–liquid interface energy of the $CuAl_2$ phase shows no dependency between the Cu concentration and the solid–liquid interface energy.

5.5 Summary and Conclusions

The radial heat flow apparatus in combination with the "grain boundary groove in an applied temperature gradient" method can be applied to measure the Gibbs–Thomson coefficient, Γ, and the solid–liquid interface energy, σ_{SL}, for grain boundary grooves in alloys where the groove shapes can be investigated after quenching. In this method, the local curvature of the grain boundary grooves and the local undercooling by heat flux simulations must be determined using the Gibbs–Thomson equation. For the simulation of the local undercooling, the temperature gradients in the liquid and the solid phases must be known in addition to the groove shape. The accuracy of the determined solid–liquid interface energy depends on many factors such as the temperature gradient, G_S, the processing time, the purity of the ingot material, the accuracy of the material-specific thermophysical data such as the thermal conductivity and the specific entropy change per unit volume.

Further sources of errors could be from the preparation of the samples, coordinate transformation, geometrical evaluation, and temperature field simulation. Owing to the segregation-induced variation of the concentrations along the height of each sample, grain boundary grooves of the $Al_{(\alpha)}$, $CuAl_2$, and Ag_2Al phase in equilibrium with the liquid phase could be observed. Finally, the average values of the solid–liquid interface energy (millijoule mJ/per square m^{2}eter) and the concentration of Cu (wt%) in the liquid phase were compared for the individual samples. From the obtained results it could be concluded that, within the margin of error, for the $Al_{(\alpha)}$ phase the solid–liquid interface energy decreases with increasing Ag concentration, whereas for the $CuAl_2$ phase no dependency of the solid–liquid interface energy on the Cu concentration could be observed for the investigated range of alloy composition.

Acknowledgments

This work was supported by the DFG (German Research Foundation) within the frame of the SPP1120 "Phase Transformations in Multicomponent Melts". The authors are grateful for the financial support.

References

1 Jones, D.R.H. and Chadwick, G.A. (1971) *Journal of Crystal Growth*, **11**, 260.
2 Jones, D.R.H. (1978) *Philosophical Magazine*, **27**, 569.
3 Schaefer, R.J., Glicksman, M.E. and Ayers, J.D. (1975) *Philosophical Magazine*, **32**, 725.
4 Hardy, S.C. (1977) *Philosophical Magazine*, **35**, 471.
5 Nash, G.E. and Glicksman, M.E. (1977) *Philosophical Magazine*, **24**, 577.
6 Bolling, G.F. and Tiller, W.A. (1960) *Journal of Applied Physics*, **31** (8), 1345.
7 Singh, N.B. and Glicksman, M.E. (1989) *Journal of Crystal Growth*, **98**, 573.
8 Bayender, B., Maraşli, N., Cadirli, E., Sisman, H. and Gündüz, M. (1998) *Journal of Crystal Growth*, **194** (1), 119.
9 Bayender, B., Maraşli, N., Cadirli, E. and Gündüz, M. (1999) *Materials Science And Engineering A*, **270**, 343–48.

10 Maraşli, N., Keşlioğlu, K. and Arslan, B. (2003) "Solid-liquid interface energies in the succinonitrile and succinonitrile-carbon tetrabromide eutectic system". *Journal of Crystal Growth*, **247**, 613–22.

11 Gündüz, M. (1984) *The Measurement of Solid-Liquid Surface Energy*, Ph.D. thesis, University of Oxford.

12 Gündüz, M. and Hunt, J.D. (1985) "The measurement of solid-liquid surface energy in the Al-Cu, Al-Si and Pb-Sn systems". *Acta Metallurgica*, **33** (9), 1651–72.

13 Gündüz, M. and Hunt, J.D. (1989) "Solid-liquid surface energy in the Al-Mg system". *Acta Metallurgica*, **37** (7), 1839.

14 Maraşli, N. (1994) *The Measurement of Solid-Liquid Surface Energy*, Ph.D. thesis, University of Oxford.

15 Maraşli, N. and Hunt, J.D. (1996) "Solid-liquid surface energies in the Al-$CuAl_2$, Al-$NiAl_3$ and Al-Ti systems". *Acta Materialia*, **44**, S1085.

16 Keşlioğlu, K. (2002) The Measurement of Solid-Liquid Surface Energy, Ph.D. Thesis, Erciyes University.

17 Keşlioğlu, K. and Maraşli, N. (2004) "Solid-liquid interfacial energy of the eutectoid b phase in the Al-Zn eutectic system". *Material Science and Engineering A*, **369**, 294–301.

18 Erol, M., Maraşli, N., Keşlioğlu, K. and Gündüz, M. (2004) "Solid-liquid interfacial energy of bismuth in the Bi-Cd eutectic system". *Scripta Materialia*, **51**, 131–36.

19 Witusiewicz, V.T., Hecht, U., Fries, S.G. and Rex, S. (2005) "The Ag-Al-Cu system II. A thermodynamic evaluation of the ternary system". *Journal of Alloys and Compounds*, **387**, 217–27.

20 Parker, W.J., Jenkins, R.J., Butler, C.P. and Abbott, G.L. (1961) "Flash method for determining thermal diffusivity". *Journal of Applied Physics*, **32**, 1679.

21 Bräuer, G., Dusza, L. and Schulz, B. (1992) "The new laser flash equipment LFA-427". *Interceram*, **41**, 7.

22 Dusza, L. (1996) *Wärmetransport–Modelle zur Bestimmung der Temperaturleitfähigkeit von Werkstoffen mit der instationären Laser Flash Methode*, Wissenschaftlicher Bericht FZKA 5820, Forschungszentrum Karlsruhe GmbH.